Available online at www.sciencedirect.com
SCIENCE DIRECT
Catalysis Today 110 (2005) 211–220
CATALYSIS TODAY
www.elsevier.com/locate/cattod

Performances of Fe-[Al, B]MFI catalysts in benzene hydroxylation with N_2O The role of zeolite defects as host sites for highly active iron species

G. Centi [a], S. Perathoner [a,*], F. Pino [a], R. Arrigo [a], G. Giordano [b], A. Katovic [b], V. Pedulà [b]

[a] *Department of Industrial Chemistry and Engineering of Materials, University of Messina, Salita Sperone 31, 98166 Messina, Italy*
[b] *Department of Chemical Engineering and Materials, University of Calabria, Italy*

Abstract

The catalytic performances of Fe-[Al, B]MFI zeolites in benzene hydroxylation with N_2O are studied as a function of the nature of the T atom (Al, B) and compared with the characterization of the nature of iron species determined by UV–vis diffuse reflectance spectroscopy. The results indicate that the mechanism for generation of iron species highly active in this reaction is the creation of hydroxyl nests in the zeolite framework due to framework to extra-framework migration of the T atom. The process is favoured when B is present as T atom, but occurs also in the case of Fe and Al as T atoms. Iron atoms migrate to these zeolite defect sites forming highly active Fe^{3+} isolated species in square pyramidal or highly distorted octahedral coordination. The process occurs during the catalyst pre-treatment as well as during the initial half an hour of time on stream, leading to an increase in the phenol productivity during this step. A model of these active sites is presented. The effect of the silica source in the preparation of these catalysts is also reported.

Keywords: Phenol; Benzene; Zeolite defects; N_2O; Fe/MFI; Boron

1. Introduction

Fe-ZSM-5 shows remarkable performance in N_2O decomposition or reduction with hydrocarbons (propane, isobutane), and in its use as selective oxidant for the benzene direct hydroxylation to phenol. The latter reaction can be considered the first example of a successful gas phase direct hydroxylation of an aromatic compound [1] and an interesting example of an eco-efficient chemical process (reuse of a byproducts having high greenhouse gas effect to improve productivity). Starting from the independent discovery from three research groups [2–4] that MFI-type zeolites selectively catalyze the reaction of N_2O with benzene to give phenol, several research groups have investigated this reaction and discussed the mechanism of reaction ([5] and references therein). However, still great debate is present regarding the nature of the iron sites responsible of the unique reactivity properties, even if sometimes confusion could derive from the fact that the active sites in the three cited reactions may be not the same.

Limiting to the reaction of benzene direct hydroxylation to phenol, different type of active sites have been indicated to be responsible for the reaction, including iron- or non-iron sites (extra-framework Al^{3+} ions, Brønsted or Lewis acid sites) ([6] and references therein). However, there is consensus recently that Fe is necessary for the reaction. The activity of samples not containing iron could derive from the presence of traces of iron due to the modalities of preparation [7]. Nevertheless, different types of iron species have been proposed in literature to be active in this reaction, such as binuclear Fe complexes [8,9], isolated Fe^{II} species with one or two Al atoms in the immediate

* Corresponding author. Fax: +39 090 391518.
E-mail address: perathon@unime.it (S. Perathoner).

0920-5861/$ – see front matter © 2005 Elsevier B.V. All rights reserved.
doi:10.1016/j.cattod.2005.09.041

vicinity [10], and iron-oxo species [11]. Together with framework (FW) iron sites in tetrahedral coordination, iron species in extra-framework (EFW) position are present and it is generally accepted that the latter species are those active in benzene hydroxylation with N_2O. However, different type of EFW iron species were evidenced to be present in Fe/MFI catalysts: (i) isolated Fe^{III} ions in different locations in the zeolite cages (indicated as α, β and γ positions [12]), (ii) isolated Fe^{II} ions [10], (iii) binuclear complexes [8], and (iv) iron-oxide nanoparticles [13]. Recently, it was also indicated that nano-oxide clusters of random structure (''ferrihydrate'') are active in phenol synthesis, but these species transform to magnetite (partially active) or hematite (inactive) iron-oxide particles [14].

The identification of the active species in these catalysts is quite difficult, due to the presence of various iron species and the low amount of iron present in these catalysts. In addition, some results pointed out that probably the most abundant iron species present in the catalyst (therefore, probably those detected by spectroscopic methods) are not those active, or the most active [15,16].

We have thus approached the problem from a different perspective. Our previous studies pointed out the possible importance of the presence of defect sites (hydroxyl nests) in the zeolite [15]. During (hydro)thermal pretreatment of the zeolite, the procedure used to activate these catalysts, some of the Al or Fe moves from framework to extra-framework positions [17,18], leaving defect zeolite sites. Iron, in extra-framework position, during the (pre)treatment as well during catalytic reaction may partially migrate into these positions, but only forming a part of the bonds, being stabilized in a pseudo-square pyramidal coordination. This is related to the fact that the position of FW Fe and Al is different in MFI structure and that the near lying EFW Al stabilizes the iron in this pseudo-framework (PFW) position.

In order to verify further this hypothesis, we have analyzed how to improve the generation of these defects. In Boralite (MFI structure), boron may easier move to extra-framework than Al [19], and therefore a higher number of these defects (hydroxyl nests) may be formed during activation. In addition, the weaker Brønsted acidity of B instead of Al as T atom [20] may also allow to eventually check whether Brønsted acidity is important in the reaction mechanism, as often suggested in the literature both in relation to the reaction mechanism [21] and the stabilization of the active iron species [22].

Panov et al. [23] have already investigated B-MFI, Ti-MFI, Ga-MFI, and Al-MFI samples, but they arrived to the conclusion that the activity is depending only on the number of α-oxygen sites, which they associated to the presence of binuclear iron species [24]. However, they observed that the nature of T atom influences also the relationship between the amount of iron and concentration of α-oxygen sites, evidencing that the mechanism is more complex, in agreement with recent data on the kinetics of N_2O decomposition [25,26]. It should be also remarked that Zholobenko [27] and Kustov et al. [28] have associated the formation of α-oxygen sites to defect zeolite sites. Therefore, a re-examination of the role of the presence of B in Fe-MFI type catalysts for benzene selective hydroxylation to phenol is useful to further contribute to the understanding of the nature of the active sites in this reaction.

2. Experimental

2.1. Catalyst preparation

The Fe-[B, Al]MFI samples were synthesized by hydrothermal method in a static Teflon®-lined autoclave and under autogeneous pressure at 170 °C. The molar composition of the starting hydrogel was xNa$_2$O-yTPABr-zAl$_2$O$_3$-rH$_3$BO$_3$-SiO$_2$-qFe$_2$O$_3$-pH$_3$PO$_4$-20H$_2$O, where $x = 0.1 - 0.3$; $y = 0.08$; $z = 0.0 - 0.05$; $r = 0.0 - 0.03$; $q = 0.0 - 0.025$; $p = 0.03$.

The synthesis procedure was the following: sodium aluminate and/or H_3BO_3 was added to a sodium-hydroxide solution and then after homogenization the organic compound (TPABr) and the silica source (silica-gel BDH or silica fumed 390) were added. A solution of an iron complex with ortophosphoric acid, starting from iron nitrate and the acid, prepared in another beaker was slowly added to the hydrogel. After 1 h of homogenization the mixture was transferred into the autoclave. For the synthesis of the silica form, the procedure was identical but without the introduction of the aluminium source. The template was removed by calcination in air up to 550 °C. The temperature was increased slowly up to the final value (from r.t. to 350 °C at a rate of 3 °C/min, then isothermal for 2h, then a further increase in temperature at a rate of 5 °C/min up to 550 °C followed by 5h in isothermal conditions at 550 °C).

The [Al]MFI samples was instead prepared from a commercial ZSM-5 sample (Alsi-Penta, Si/Al = 50, SN 27 in the NH_4^+ form) by controlled thermal treatment (calcinations at 550 °C).

The solid products either after synthesis or after template removal were analyzed by powder X-ray diffraction (XRD), infrared spectroscopy (FT-IR), BET surface area measurements and scanning electron microscopy (SEM) to verify the synthesis procedure and crystallinity of the samples. In all cases, only MFI zeolite structure was detected to be present. No evidences were found for other crystalline phases, including the presence of iron-oxide. Table 1 summarizes the characteristics of the sample prepared.

Table 1
Characteristics of different catalysts

Code	Si/Al	Si/B	Fe (wt.%)	Silica source[a]	Surface area (m^2/g)
Fe-MFI	–	–	2.21	SF	391
Fe-[Al]MFI	50	–	2.11	SF	372
Fe-[B]MFI	–	50	2.06	SF	425
Fe-[B, Al150]MFI[b]	150	50	2.08	SF	386
$Fe_{3.1}$-[B, Al152]MFI	152	50	3.05	SF	394
Fe-[B, Al76]MFI	76	50	2.05	SF	406
Fe-[B, Al150]MFI SG	150	50	2.12	SG	441

[a] SG: silica fumed 390; SG: silica gel BDH.
[b] Alternative indications in the text: $Fe_{2.1}$-[B, Al150]MFI, Fe-[B, Al150]MFI SF.

2.2. Catalytic tests

The catalytic tests in selective oxidation of benzene to phenol using N_2O as the oxidant were made in a fixed-bed reactor at 400 °C feeding a mixture containing 20% benzene and 3% N_2O in helium. These reaction conditions correspond to a good compromise between high productivity to phenol and stability of the catalytic behavior. The influence of the reaction temperature, benzene and N_2O concentration was analyzed, but will be not reported here, because do not significantly affect the comparison between the catalysts performances.

The total flow rate was 3 l/h and the amount of catalyst was 0.5 g (contact time of 0.6 s g/ml). The catalysts were used in the forms of powder. It was verified by analyzing the dependence of the catalytic performances from the linear gas-velocity (at constant contact time) and from the particle diameter that in these reaction conditions inter- and intra-phase mass and heat transfer limitations do not influence markedly the comparison of the catalysts performances. Further calculations (β factor, Biot number) supported this conclusion.

The feed was prepared using an already calibrated mixture of N_2O in helium and adding benzene using an infusion pump and a vaporizer chamber. The feed could be sent either to the reactor or to a by-pass for its analysis. The feed coming out of the reactor or from the bypass could be sent to vent or to one of two parallel absorbers containing pure toluene as the solvent (plus calibrated amounts of tetrahydrofuran as the internal standard) cooled at about −15 °C in order to condense all organic products. The line to the absorbers was heated at about 200 °C in order to prevent condensation of the products. The vent, after condensation of the organic products, was sent to a sampling valve for analysis of the residual gas composition. The reactor outlet stream was sent alternatively to the two parallel absorbers for a given time (typically 5 min), in order to monitor the change in the catalytic activity averaged over this time.

N_2O, O_2, N_2 and total oxidation products (CO and CO_2) were analyzed using TCD-Gas chromatography and a 60/80 Carboxen-1000 column, whereas benzene and phenol (as well as other minor aromatic by-products) were determined by FID-Gas chromatography using a ECONO-CAP SE-30 ''wide bore'' column or a Mass-GC equipped with a capillary Chrompack CP-Sil 5CB-MS Fused Silica column.

The catalytic results will be presented here in terms of phenol productivity (PP; millimoles per hour per g of catalyst) and selectivity (PS) with respect to the gas-phase products of reaction. Carbon oxides were the main products of reaction together with phenol. Only traces of other products were detected.

Before the reactivity tests the catalysts were activated in situ at 700 °C in a flow of helium.

2.3. Characterization

The BET surface area was measured using N_2 sorption at 77 K. Prior to the experiments, the samples were outgassed at 120 °C for 3 h. X-ray powder diffraction patterns were collected using Cu Kα radiation, on a Ital-structures XRD diffractometer. Diffuse reflectance (DR) UV–vis experiments were carried out on powdered samples using a Jasco V570 spectrometer equipped with an integrating sphere for solid samples. The reference was $BaSO_4$ and the spectra were recorded in air at room temperature. Spectra deconvolution was made using a spectral deconvolution software and assuming a Gaussian line shape.

The size and morphology of the crystals were studied with a scanning electron microscope Jeol 5600 LV. Thermogravimetric (TG) tests to analyze the amount and the characteristics of the carbonaceous species formed during the catalytic reaction were made in a TGA Q50 apparatus (TA Instruments). The samples were discharged from the reactor for catalytic tests after flushing with helium for 5 min at the same temperature of the catalytic tests (400 °C), in order to remove weakly adsorbed species. TG tests were made in a flow of air (60 ml min^{-1}), which passes tangential to the pan of the TG apparatus containing approximately 3–4 mg of sample. The heating rate was 5 °C/min from r.t. (25 °C) to 1000 °C. The samples after the TG experiments turned from black to white, indicating complete removal of carbonaceous species.

3. Results and discussion

3.1. The role of B as T atom in MFI zeolites

Reported in Fig. 1 is the comparison of the dependence of the phenol productivity (PP) from the time on stream during catalytic tests at 400 °C on the following samples: iron-silicalite (Fe-MFI), iron-aluminium-silicalite (Fe-[Al]MFI) and iron-boron-silicalite (Fe-[B]MFI). All these samples were synthesized under comparable reaction conditions, calcined in air and then activated in situ prior to the catalytic tests using the same procedure. In addition, the Si/M ratio and the amount of iron in the sample was similar (see Table 1). Therefore, they allow to understand if the catalytic performances depend on the presence and nature of the T-atom in the MFI-type zeolite.

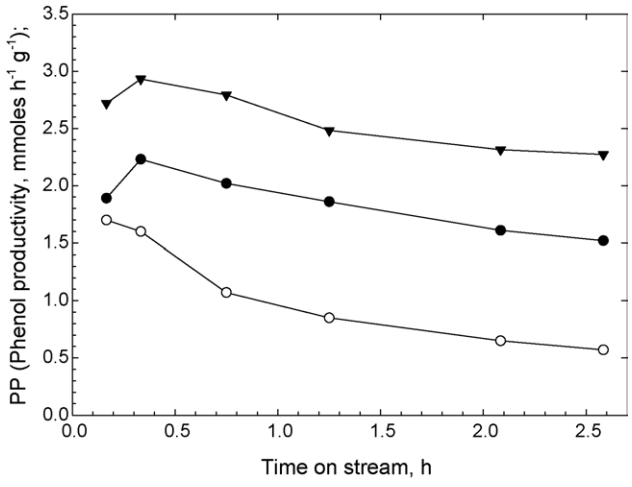

Fig. 1. Phenol productivity (PP) at 400 °C as a function of the time-on-stream for different catalysts: (○) Fe-MFI; (●) Fe[Al]MFI; (▼) Fe[B]MFI.

While the selectivity to phenol do not depend significantly on the time on stream and the nature of the catalyst (it was always in the 90–98% range), large variations were observed regarding the phenol productivity. Initial productivity in Fe-MFI (iron-silicalite) was around 1.7 mmol h^{-1} g^{-1} and progressively decreases to a value around one third in 3 h of time on stream. In Fe-[Al]MFI (Fe-ZSM-5), the starting productivity was similar to that of Fe-MFI, but instead to decrease, an initial increase of the activity was observed during the first half an hour. Note, that instead the selectivity to phenol does not change. After this maximum, the productivity decreases regularly and after three hours of time on stream, the phenol productivity is around 2.5 times higher than that of Fe-MFI. This is consistent with the results of Panov et al. [23] and other literature data, which indicate that the presence of Al in the zeolite framework leads to higher catalyst performances.

When B is present in the zeolite framework instead of Al, the general trend is similar, but the initial phenol productivity is significantly higher (2.7 mmol h^{-1} g^{-1} for Fe-[B]MFI with respect to 1.7 mmol h^{-1} g^{-1} for Fe-[Al]MFI). After three hours of time on stream, Fe-[B]MFI phenol productivity remains higher than that of Fe-[Al]MFI, pointing out that the rate of catalyst deactivation is similar, but the number of active sites in Fe-[B]MFI was higher than in Fe-[Al]MFI.

Thermogravimetric tests of oxidation of the carbon deposited on these catalysts after 3 h of time on stream during benzene oxidation with N_2O do not indicate marked differences between the amount of carbon present (ranging in the 4–6 wt.% range) and its temperature of oxidation (oxidation in the 350–450 °C temperature range). XRD and IR characterization of these three samples before and after the catalytic tests also do not indicate marked differences in the zeolite crystallinity, neither the amorphization of the samples during the catalytic tests. The measurements of the surface areas of these samples (Table 1) and of their porosity also do not provide evidences about marked differences between the samples. Therefore, the different catalytic performances should be attributed to a different amount of active iron species, and/or the presence of iron sites having higher intrinsic catalytic activity in benzene direct hydroxylation.

Fig. 2a reports the comparison of the UV–vis diffuse reflectance spectra of these samples and for comparison that of [Al]MFI (ZSM-5). It may be noted that pure silicalite has no bands in this region and also the weak bands of commercial [Al]MFI (ZSM-5) at about 210 and 250 (shoulder) nm (spectrum 4 in Fig. 2) are due to M ← O charge-transfer (CT) bands of impurities (mainly iron impurities, present in a concentration of about 200 ppm and responsible of the catalytic behavior of [Al]MFI in benzene hydroxylation with N_2O [6,29]).

In Fig. 2b the deconvolution of a spectrum (spectrum 3) is also reported in order to better clarify the envelope of bands forming the overall spectrum. The deconvolution was made according to the method reported by Perez-Ramirez et al. [30]. For isolated Fe^{3+} sites, two CT ($Fe^{3+} \leftarrow O^{2-}$) bands associated to $t_1 \rightarrow t_2$ and $t_1 \rightarrow e$ transitions are expected at about 215 and 240 nm for tetrahedral coordination such as in pure iron-silicalite [31] and at slightly higher wavelength (about 250 and

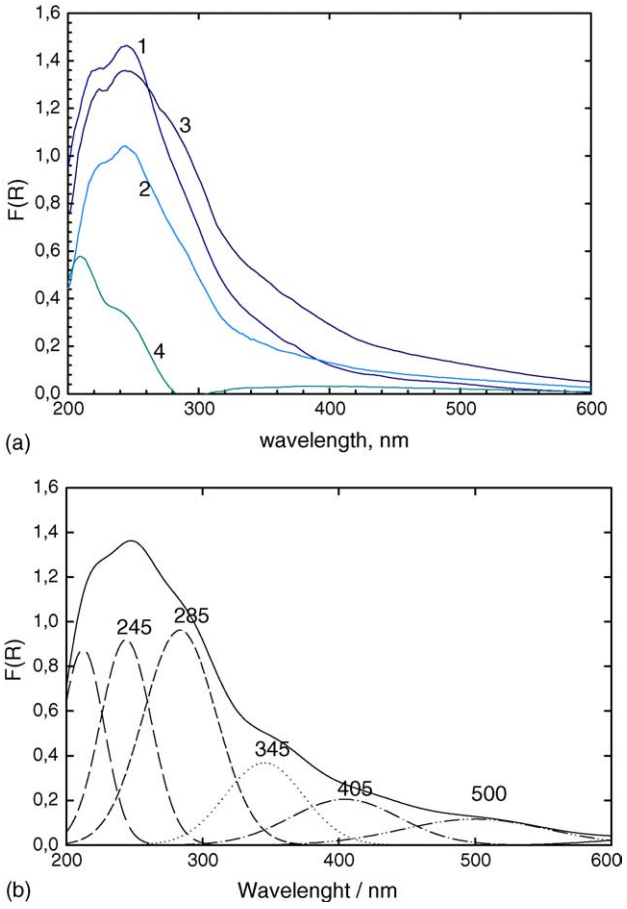

Fig. 2. (a) UV–vis DR spectra for Fe[B]MFI (1); FeMFI (2); Fe[Al]MFI (3); [Al]MFI (4) catalysts recorded before hydrothermal pre-treatment. (b) Deconvolution of the spectrum of the Fe-[Al]MFI sample.

280 nm) for square-pyramidal and distorted octahedra such as for isolated ions on alumina surface [32]. More difficult is the attribution of bands at higher wavelength, which are generically attributed to CT transitions of Fe^{3+} ions in small oligonuclear clusters ($Fe_x^{3+}O_y$) (broad bands between 300 and 450 nm) and larger Fe_2O_3 particles (above 450 nm) [30,31].

Diiron-μ-oxo complexes, e.g. di-Fe^{III} complexes with a single Fe–O–Fe bridge, are characterized by LMCT (ligand-to-metal charge transfer) bands at about 330 nm and 420 nm [33]. μ-Oxo bridged dinuclear iron 1,10 phenantrhroline complex encapsulated in MCM-41 also shows an adsorption at 320 nm assigned to $p_{x(O)} \rightarrow d_{xy(Fe)}$ transition (charge transfer from the oxygen to Fe orbital) which is absent in the monomeric complex [34]. Binuclear oxo-bridged iron(III) complexes of chiral tetradentate ligands [35], e.g. having a Fe–O–Fe bridge and a Fe–O–CO–O–Fe bridge, are characterized from an oxo-Fe^{3+} CT band near 370 nm and a second less intense transition near to 470 nm. In dinuclear iron complexes in hexagonal mesoporous solids having both a Fe–OH–Fe bridge and a Fe–OR–Fe bridge [36], a shoulder near 380 nm could be detected which shifts to about 430 nm by reaction with peroxides forming a μ-peroxo intermediate. In dinuclear iron(III) complexes having both μ-hydroxo or μ-oxo and μ-peroxo bridges (e.g. both Fe–O(H)–Fe and Fe–O–O–Fe

bridges), an intense peroxo LMCT band at about 580 nm is observed (μ-oxo and μ-peroxo) which shifts to about 645 nm upon protonation [37].

It may be concluded that the LMCT band of single Fe–O–Fe oxo bridges in dinuclear iron(III) clusters is expected near to 330 nm (with a weaker transition near to 420 nm) shifting to lower energies (about 50–80 nm) upon protonation or when a second oxo-bridge is present. Peroxo bridges are instead falling at lower energies, in the 550–600 nm region. It should be noted, however, that in this region (300–580 nm) bands are also expected for iron hydroxide, ferrihydrite oxide and/or defective iron-oxide nanoparticles, while larger iron-oxide (hematite) particles (with mean diameter above around 20–50 nm) show an adsorption band near 580 nm. In fact, it has been reported that (i) β-FeOOH nanoparticles (2–5 nm) in a macroporous resin give rise to a broad and weak band near 430 nm assigned to double-exciton process of Fe-Fe pairs [38], (ii) nanoparticles (5 nm) of ferrihydrite oxide give rise to an absorption near 300–350 nm [39], and (iii) highly electron deficient iron-oxide nanoparticles intercalated in layered compounds also give rise to bands near 350 and 450 nm [40].

Based on these considerations, it is possible to analyze the effect of the T atom (B, Al) on the nature of the iron species present in the catalysts (Fig. 2a). The spectrum of Fe-MFI (iron-silicalite, spectrum 2 in Fig. 2a) is characterized by two intense bands at about 215 and 245 nm related to $t_1 \rightarrow t_2$ and $t_1 \rightarrow e$ CT transitions of framework Fe^{3+} ions (tetrahedral coordination), and a long tail in the lower energy side which could be deconvoluted in at least two components at about 285 and 350 nm. The intensity of these bands increases as a function of the temperature of thermal treatment and, in agreement with literature data, could be assigned to LMCT bands of isolated or dimeric extra-framework Fe^{2+} species, and/or ferrihydrite oxide nanoparticles. The latter species was shown to be present in Fe-MFI by ESR and Mössbaurer spectroscopies [15]. When B is present in the framework, the spectrum does not changes significantly, but it is more intense (note that the amount of iron in these samples is nearly the same). This was systematically observed also in other samples. As observed above, for isolated Fe^{3+} in square-pyramidal or highly distorted octahedral coordination, as expected for iron ions located in hydroxyl nests generated by migration of the T atom (boron) from framework (FW) to extra-framework (EFW) position, these two bands shift of about 20–30 nm to lower frequencies, but their extinction coefficient is expected to be higher than that of tetrahedral iron sites (framework), due to the less symmetrical coordination. Therefore, the enhanced intensity of the spectrum on Fe-[B]MFI with respect to Fe-MFI is consistent with a partial FW → EFW migration of B and the stabilization instead of iron in the hydroxyl nests generated from this process. This is reasonable, due to the better overlap of Fe and O orbitals with respect to B and O orbitals [20b,41] and the different preferable sitting for Fe and B in MFI framework [42].

In Fe-[Al]MFI (spectrum 3 in Fig. 2a) the intensity of the two bands at 215 and 245 nm only slightly decreases, but increase in intensity the bands centred near 285, 345 and 400 nm. This is consistent with the presence of EFW isolated Fe^{3+} in nearly symmetrical octahedral coordination (band near 300 nm), oxo-bridged dinuclear iron species (band near 350 nm) and FeOOH or ferrihydrite oxide nanoparticles (bands in the 350–500 nm region). Although unambiguous attribution is not possible, UV–vis DR spectra of Fe-[B]MFI and Fe-[Al]MFI clearly evidence a different nature and/or distribution of iron species in these two samples, with the presence of species having higher nuclearity in Fe-[Al]MFI and probably the presence of differently coordinated isolated Fe^{3+} sites.

This interpretation is consistent with literature data. Fe K-edge XANES results [43] showed a distinct difference in the characteristics of iron in Fe-silicalite (without aluminium) and FeZSM-5 (with aluminium), in agreement with UV–vis DR data (Fig. 2). The presence of a large amount of higher nuclearity species in Fe-[Al]MFI with respect to Fe-[B]MFI agrees with the results of Dedecek et al. [44]. These authors, studying the effect of the type of isomorphously substituted (IS) atoms (Al, Fe, B) on the number of isolated IS atoms (IS–Si $n \geq 3$-IS) and their pairs (IS–Si–IS and IS–Si–Si–IS), and on the distribution of these IS pairs in the framework of ZSM-5 structure prepared under the same reaction conditions, evidenced that the distribution of IS atoms (Al, Fe, B) in the ZSM-5 framework is not random and depends on the type and concentration of the IS atom. The number of pairs of B is significantly lower compared to the number of Al or Fe pairs in the ZSM-5 matrix of similar Si/IS ratio.

It should be finally mentioned that Mössbauer data [15] indicate that the amount of Fe^{2+} in calcined Fe-MFI samples, as those reported in Fig. 2a, is nearly negligible and for this reason the presence of these sites was not accounted in the interpretation of spectra reported in Fig. 2a. However, during the catalytic tests these Fe^{3+} species could be reduced to Fe^{2+} ions. Mössbauer data indicate the presence of Fe^{2+} ions after the catalytic tests on Fe-MFI samples [15]. Therefore, limiting discussion to the Fe^{3+} species in the calcined samples do not imply that Fe^{2+} species could be those active (as suggested by various authors in the literature), because these reduced iron species could form in situ during the catalytic tests.

3.2. The role of B on the formation of highly active iron sites

Comparing the results of UV–vis DR characterization (Fig. 2) with those of the catalytic behavior (Fig. 1) it is possible to derive some conclusion about the relationship between the nature of the iron species and the catalytic behavior, although limited to the initial activity, because due to the formation of carbonaceous deposits during the reaction, the analysis of the change of the UV–vis DR spectra as a function of the time on stream, was not possible.

Fig. 3 reports the relationship observed between the area of the bands at about 212, 245, 285 and 345 nm in the samples (obtained by spectra deconvolution) and the initial productivity to phenol. Even taking into account the limits deriving from spectral deconvolution, a linear relationship is observed between the intensity of the bands at about 212 and 245 nm and the phenol initial productivity. No correlation is instead

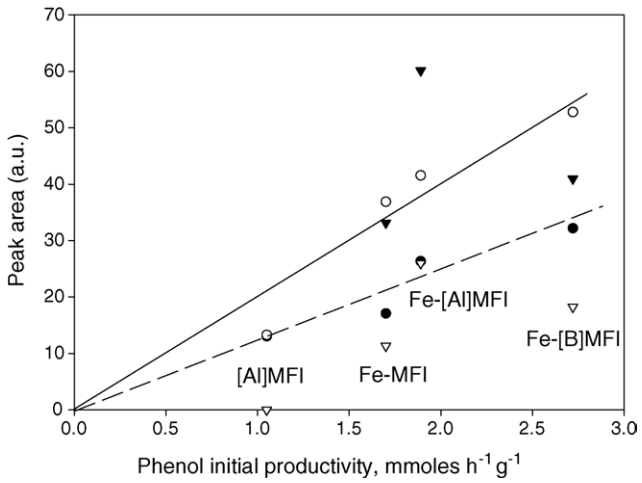

Fig. 3. Relationship between the area of the bands at 212 (●), 245 (○), 285 (▼) and 345 nm (▽) (obtained by the deconvolution of the spectra reported in Fig. 2a; see text) and the phenol initial productivity during reactivity tests at 400 °C.

observed for the other two bands, as well as for the bands at higher wavelength (>350 nm).

As discussed before, the bands at 212 and 245 nm are usually attributed to FW Fe^{3+} ions, but there are several evidences that these ions are essentially inactive in benzene hydroxylation with N_2O. To clarify this apparent contradiction, it should be noted that in iron-silicalite samples with low amount of EFW iron, the 212 nm band is around two times more intense than that at about 245 nm, similarly to the spectrum of [Al]MFI sample, but differently from other samples reported in Fig. 2. This is related to the overlap of the $t_1 \rightarrow e$ CT transition of framework Fe^{3+} ions with the $t_1 \rightarrow t_2$ transition of isolated Fe^{3+} ions in square pyramidal or distorted octahedral coordination. Due to the asymmetric environment of the latter ions, other LMCT bands are also expected at higher energy, thus overlapping with the 212 nm band. The band near 245 nm may be thus indicative of the presence of Fe^{3+} ions in square pyramidal or distorted octahedral coordination, while the bands at higher wavelength (285 and 345 nm) are indicative of the presence of octahedral isolated iron species and oxo bridges between two iron ions (dimeric species or FeOOH or ferrihydrite oxide nanoparticles), respectively. The results reported in Fig. 3 therefore indicate that no unique relationship may be observed between species characterized from the presence of oxo bridges between two iron species such as iron dimers, and probably also between isolated octahedral Fe^{3+} species, while a relationship could be indicated for isolated Fe^{3+} ions in square pyramidal or highly distorted octahedral coordination. This suggests that the latter species are more active in the benzene direct hydroxylation with N_2O, although do not exclude that the other species are also active in the reaction.

It may be concluded, that the analysis of the role of B as T atom in MFI zeolites indicates that the mechanism to generate iron species highly active in benzene hydroxylation with N_2O consists in the creation of hydroxyl nests in zeolite framework due to FW to EFW migration of the T atom. The process is favoured when B is present as T atom, but occurs also in the case of Fe and Al as T atoms. ^{29}Si-NMR data [15] confirm the presence of such zeolite defects, which decrease after the catalytic tests. Iron atoms may migrate to these zeolite defect sites (silanol nest reoccupation of deboronated MFI is known to occurr [19b]) forming highly active Fe^{3+} isolated species in square pyramidal or highly distorted octahedral coordination, although the other iron species present are also probably active in the reaction. In iron–boralite samples, the easier process of deboronation as well as the different localization of B in the framework (with respect to Al) maximizes the formation of these isolated Fe^{3+} species in square pyramidal or highly distorted octahedral coordination, leading therefore to more active catalysts. The migration of Fe from FW to EFW position and then to PFW (pseudo-framework) position is reasonable taking into account that the sitting of FW Fe and Al is different in MFI structures [44] and that the near lying EFW Al or B stabilizes the iron in this pseudo-framework (PFW) position [43].

Although the exact nature of the iron in this pseudo-framework (PFW) position should be better clarified by further studies, the difference between iron framework (Fe_{FW}) and iron pseudo framework (Fe_{PFW}) position related to the different preferable position of Fe and Al or B T atoms in ZSM-5 zeolite framework [42]. Therefore, in the process of migration of iron from framework to extra-framework and then reinsertion in defect sites created from B or Al extra-framework position, the local coordination environment around iron atoms is different. In addition, the strong electrostatic field created by nearlying Al or B extra-framework atoms is suggested to stabilize a different coordination of the iron atoms, and specifically a Fe^{2+}=O square pyramidal species [15]. It is interesting to observe that Koningsberger et al. [45] evidenced by X-ray absorption near-edge spectroscopy the formation of three-coordinate aluminium in ZSM-5, which is in good agreement with the mechanism suggested above.

During the first half an hour of time on stream this process of relocation of iron ions from EFW to zeolite defects forming more active species continues. This could explain the initial activation of the samples and why this effect is present when a different T atom (with respect to Fe) is present in the zeolite, although some other effects (such as the initial reduction of Fe^{3+}) may also simultaneously occur.

It should be finally noted that notwithstanding the different Brønsted and Lewis acidity of the samples, related to the presence of B or Al as T atoms, no difference was observed regarding the rate of deactivation of the catalyst (Fig. 1), as well as in the amount of carbon deposit after 3 h of time on stream. This indicates that the rate of deactivation does not significantly depend on the acidity of the zeolite.

3.3. Catalytic behavior of Fe-[B, Al]MFI samples

In order to further analyze the role of B in promoting the catalytic performances in benzene hydroxylation, zeolites containing the three T atoms (Fe, B, Al) were also prepared and tested. Reported in Fig. 4 are the results obtained for samples having all the same content of B, but increasing amount of Al: only traces (Fe-[B]MFI), a Si/Al ratio of 150 (Fe-[B, Al150]MFI)

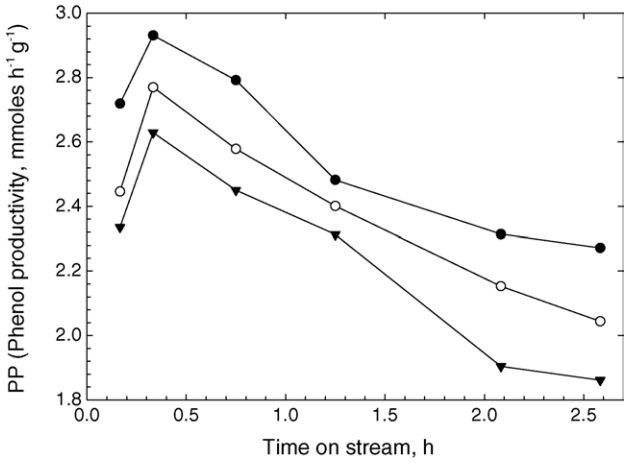

Fig. 4. Phenol productivity (PP) at 400 °C as a function of the time on stream for Fe-[B]MFI (●), Fe-[B, Al150]MFI (▼) and Fe-[B, Al76]MFI (■) catalysts.

and a Si/Al ratio of 76 (Fe-[B, Al76]MFI). The general trend of the phenol productivity in these three samples as a function of the time on stream is similar, but the phenol productivity decreases on increasing the content of Al in the samples.

The presence of Al stabilizes B with respect to the migration to EFW position [46–48] and therefore increasing the Al content in the sample, a decrease in the generation of hydroxyl nests and highly active iron species may be expected. The catalytic results reported in Fig. 4 are therefore consistent with the mechanism of generation of highly active iron species discussed before.

The effect of the amount of iron was also analyzed. Reported in Fig. 5 is the catalytic behavior of two Fe-[B, Al150]MFI samples having a content of iron of 2.1 and 3.1%, respectively. Increasing the amount of iron, (i) a decrease in the phenol productivity and selectivity and (ii) an increase in the rate of deactivation was noted. UV–vis DR spectrum of this sample (see Fig. 5b) shows the presence of a broad tail in the spectrum in the 300–600 nm region, more intense with respect to that of the sample containing 2.1% Fe. This indicates the presence of iron-oxide nanoparticles to which the lowering of the catalytic performances may be attributed. Therefore, the maximum loading of iron in these samples to avoid the formation of iron species (leading to a lowering of the catalytic performances) is around 2 wt.%.

3.4. The effect of silica source

The silica source during the hydrothermal synthesis of the zeolites has also an effect on the catalytic performances, although mainly related to changes occurring during the first two hours of time on stream, as evidenced in Fig. 6 which also shows that there is a continuous nearly linear decrease of the productivity to phenol which reaches a value close to zero in around 15–16 h of time on stream. Whereas the utilized silica source do not influence the phenol selectivity which remains constant at about 98% with time on stream.

Using silica fumed during the synthesis of the zeolite, round-shaped and regular crystals of dimension around 1 μm are obtained (Fig. 7a). The amount of Fe and Al in the samples has

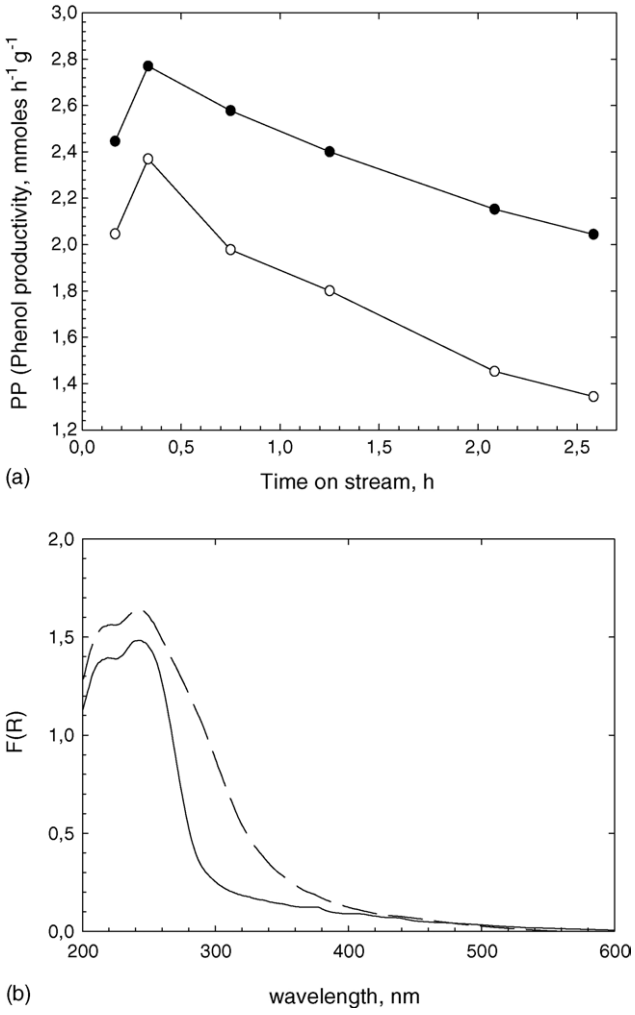

Fig. 5. (a) Phenol productivity (PP) at 400 °C as a function of the time on stream for $Fe_{2.1}$-[B, Al150]MFI (○) and $Fe_{3.1}$-[B, Al152]MFI (●) catalysts. (b) UV–vis DR spectra of these two catalysts: $Fe_{2.1}$-[B, Al150]MFI (full line) and $Fe_{3.1}$-[B, Al152]MFI (dashed line).

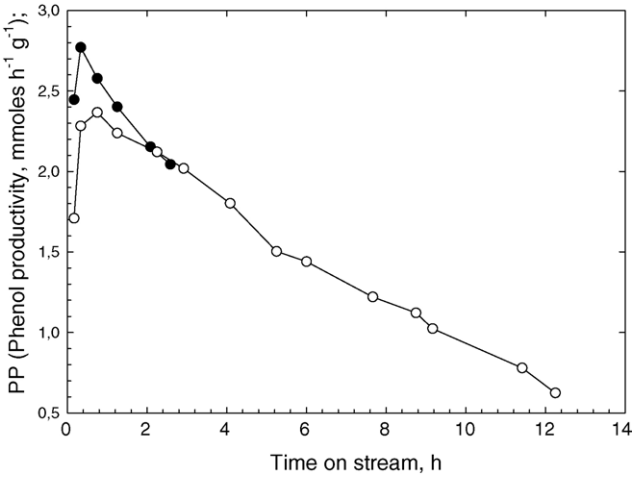

Fig. 6. Phenol productivity (PP) at 400 °C as a function of the time on stream for Fe-[B, Al150]MFI SF (●) (and Fe-[B, Al150]MFI SG (○) catalysts.

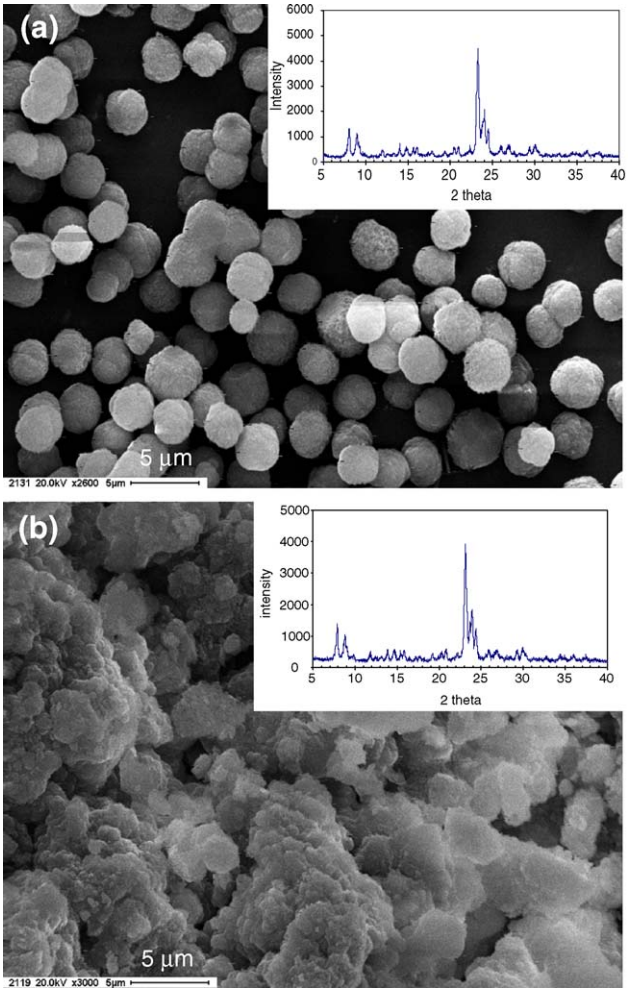

Fig. 7. SEM and XRD data for Fe-[B, Al150]MFI SF and Fe-[B, Al150]MFI SG catalysts.

some influence on the crystal dimensions, but which remain of round-shaped form. On the contrary, using silica gel as silica source, more irregular crystals were obtained (Fig. 7b). Their dimension is similar to those prepared using silica fumed (the larger particles in Fig. 7b are aggregates of smaller particles). In terms of crystallinity of the samples (see XRD in the inset of SEM micrographs), no relevant differences could be noted.

Due to the more regular crystal growth in the case of the preparation starting from silica fumed (Fig. 7a), it is probable that a more homogenous distribution of T atoms could be obtained and therefore a higher initial phenol productivity in the first hours of reaction. On the contrary, in the case of the preparation starting from silica gel, the dishomogeneous initial situation determines a more severe rearrangement, in agreement with the more drastic initial increase in the phenol productivity (from 1.7 to 2.4 mmol h^{-1} g^{-1} with respect to a change from 2.4 to 2.8 mmol h^{-1} g^{-1} for the sample prepared from silica fumed). However, further studies are necessary to clarify this aspect.

4. Conclusions

The analysis of the role of B as T atom in MFI zeolites and in particular the relationship which may be observed between initial productivity to phenol and nature of the iron species (Fig. 3), as estimated from the analysis of UV–vis DR spectroscopy data (Fig. 2), indicates that a mechanism to generate iron species highly active in benzene hydroxylation with N_2O is the creation of hydroxyl nests in the zeolite framework due to FW to EFW migration of the T atom. The process is favoured when B is present as T atom, but occurs also in the case of Fe and Al as T atoms. Iron atoms may migrate to these zeolite defect sites forming highly active Fe^{3+} isolated species in square pyramidal or highly distorted octahedral coordination, although the data do not exclude that the other iron species, which are present in the catalysts may be also active in the reaction. In iron-boralite samples, the easier process of deboronation as well as the different localization of B in the framework (with respect to Al) maximizes the formation of these Fe^{3+} isolated species in square pyramidal or highly distorted octahedral coordination, leading therefore to more active catalysts. The migration of Fe from FW to EFW position and then to PFW (pseudo-framework) position is reasonable taking into account that the sitting of FW Fe and Al is different in MFI structures and that the nearlying EFW Al or B stabilizes the iron in this pseudo-framework (PFW) position.

Based on these considerations, the model of highly active iron sites for benzene hydroxylation with N_2O reported in Fig. 8

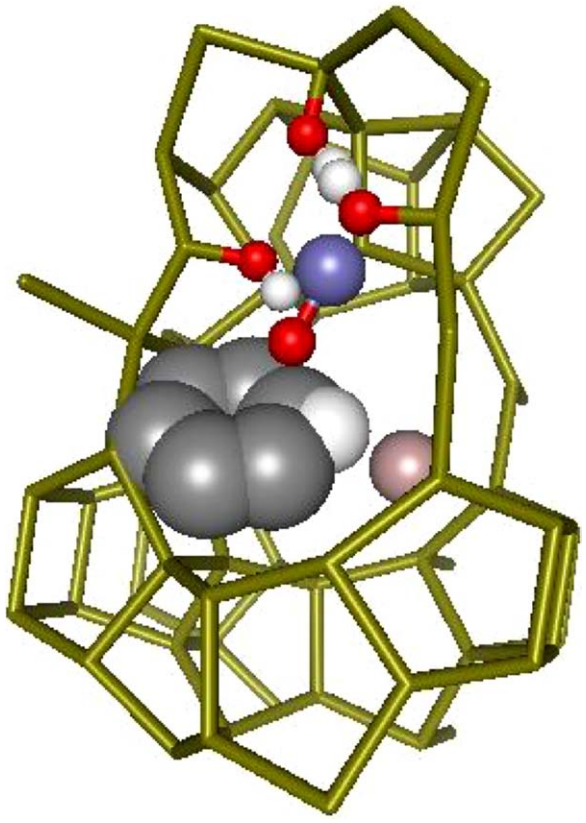

Fig. 8. Model proposed for the highly active iron sites for benzene hydroxylation with N_2O. Fe^{3+} (blue) localized in a zeolite defect site (O red and H white representing therefore hydroxyl groups in defects) near lying to EFW Al and/or B atoms. In these conditions the highly active isolated and coordinatively unsaturated Fe^{2+} species forms, as described in the text.

can be proposed. The isolated square-pyramidal iron sites in hydroxyl nests are stabilized by the presence of near lying extra-framework T atoms (Al, B), which also probably stabilizes the reaction intermediate during the hydroxylation process [49,50].

During about the first half an hour of time on stream this process of relocation of iron ions from EFW to zeolite defects forming more active species continues. This could explain the initial activation of the samples and why this effect is present when a different T atom (with respect to Fe) is present in the zeolite. At the same time, reduction of Fe^{3+} to Fe^{2+} may also occur. It was evidenced that isolated Fe^{2+} species are less affected by the steaming treatment [51] consistently with the proposed nature of the active sites. It was also reported that a noticeable part of Fe^{3+} is reduced to ferrous ions in the iron-containing aluminosilicalite, while the ferric species in the ferrosilicalite maintain their oxidation state [43]. Finally, the model is consistent with recent results [52] indicating that isolated Fe^{2+} ions characterized by high coordinative unsaturation shows the highest activity in N_2O decomposition. The adsorbed oxygen formed upon N_2O decomposition on isolated sites give rises to the formation of ferryl groups, while on oxidic clusters to bridged structures [52]. The ability to selectively oxidize benzene to phenol with nitrous oxide was related to the former sites. Probably the reaction mechanism is the following:

$$(-\mathrm{Si}-\mathrm{O})_2\mathrm{Fe}^{2+} + \mathrm{Si}-\mathrm{OH} \xrightarrow{\mathrm{N_2O}} (-\mathrm{Si}-\mathrm{O})_2\mathrm{Fe}^{4+} = \mathrm{O} \rightleftharpoons (-\mathrm{Si}-\mathrm{O})_2\mathrm{Fe}^{3+}-\mathrm{O}^-$$

in which the ferryl group is in equilibrium with the tautomeric form, the latter being the effective hydroxylating species.

In conclusion, the analysis of the effect of B as T atom in iron-MFI catalysts for benzene hydroxylation suggests that isolated Fe^{3+} located in zeolite defect sites and near to EFW T atoms (Al, B) are the precursors of the active, isolated and coordinatively unsaturated Fe^{2+} species which form in situ during the catalytic reaction upon reaction with the reactants.

References

[1] G. Centi, S. Perathoner, Selective oxidation, in: I.T. Horvath (Ed.), Encyclopedia of Catalysis, vol. 6, 2003, pp. 4230–4262.
[2] H. Gubelmann, J. Tirel, US Patent 5001280, EP Patent 0341165 (1988).
[3] A.S. Kharitonov, T.N. Alexandrova, L.A. Vostrikova, K.G. Ione, G.I. Panov, Russian Patent 4445646 (1988).
[4] E. Suzuki, K. Nakashiro, Y. Ono, Chem. Lett. 953 (1988).
[5] (a) G.I. Panov, CATTECH 4 (2000) 18;
(b) I. Yamanaka, Shokubai 46 (2004) 25.
[6] S. Perathoner, F. Pino, G. Centi, G. Giordano, A. Katovic, J.B. Nagy, Topics Catal. 23 (2003) 125.
[7] Z. Sobalik, P. Kubanek, O. Bortnovsky, A. Vondrova, Z. Tvaruzkova, J.E. Sponer, B. Wichterlova, Studies Surf. Sci. Catal. 142 (2002) 533.
[8] P. Marturano, L. Drozdova, A. Kogelbauer, R. Prins, J. Catal. 192 (2000) 236.
[9] A.L. Yakovlev, G.M. Zhidomirov, R.A. van Santen, J. Phys. Chem. B 105 (2001) 12297.
[10] G. Berlier, A. Zecchina, G. Spoto, G. Ricchiardi, S. Bordiga, C. Lamberti, J. Catal. 215 (2003) 264.
[11] K. Yoshizawa, T. Yumura, Y. Shiota, T. Yamabe, Bull. Chem. Soc. Jpn. 73 (2000) 29.
[12] Z. Sobalik, J.E. Sponer, Z. Tvaruzkova, A. Vondrova, S. Kuriyavar, B. Wichterlova, Stud. Surf. Sci. Catal. 135 (2001) 1545.
[13] G. Centi, S. Perathoner, F. Vazzana F., in: A. Bell, G. Centi, B. Wichterlowa, (Eds.), Catalysis by Unique Ion Structures in Solid Matrices, NATO., Science Series II: Mathematics, Physics, Chemistry, Kluwer/Academic Press Pub.: New York, 2001, p. 165 (Chapter 11).
[14] P. Fejes, K. Lazar, I. Marsi, A. Rockenbauer, L. Korecz, J.B. Nagy, S. Perathoner, G. Centi, Appl. Catal. A: Gen. 252 (2003) 75.
[15] G. Centi, G. Giordano, P. Fejes, A. Katovic, K. Lazar, I. Marsi, J.B. Nagy, S. Perathoner, F. Pino, Studies Surf. Sci. Catal. 154 (2004) 2566.
[16] S. Perathoner, F. Pino, G. Centi, G. Giordano, A. Katovic, J.B. Nagy, K. Lazar, P. Fejes, Stud. Catal. Surf. Sci. 142 (2002) 503.
[17] L.V. Pirutko, A.S. Kharitonov, V.N. Romenikov, A.M. Valadin, Appl. Catal. A: Gen. 138 (1997) 102.
[18] J.J. Krishnan, S. Pillai, W.M.H. Sachtler, J. Catal. 221 (2004) 119.
[19] (a) A. Cichocki, W. Lasocha, M. Michalik, Z. Sawlowicz, M. Bus, Zeolites 10 (1990) 583;
(b) R. De Ruiter, A.P.M. Kentgens, J. Grootendorst, J.C. Jansen, H. van Bekkum, Zeolites 13 (1993) 128.
[20] (a) C.T.W. Chu, C.D. Chang, J. Phys. Chem. 89 (1985) 1569;
(b) S.P. Yuan, J.G. Wang, Y.W. Li, H. Jiao, J. Phys. Chem. A 106 (2002) 8167.
[21] P.P. Nottè, Topics Catal. 13 (2000) 387.
[22] J. Pèrèz-Ramirez, G. Mul, F. Kapteijn, J.A. Moulijn, J. Catal. 207 (2002) 113.
[23] L.V. Pirutko, V.S. Chernyavsky, A.K. Uriarte, G.I. Panov, Appl. Catal. A: Gen. 227 (2002) 143.
[24] K.A. Dubkov, N.S. Ovanesyan, A.A. Shteimman, E.V. Starokon, G.I. Panov, J. Catal. 207 (2002) 341.
[25] N.A. Kachurovskaya, G.M. Zhidomirov, E.J.M. Hensen, R.A. van Santen, Catal. Lett. 86 (2003) 25.
[26] J.A. Ryder, K.A. Chakraborty, A.T. Bell, J. Catal. 220 (2003) 84.
[27] V.L. Zholobenko, Mendeleev Commun. 3 (1993) 28.
[28] L.M. Kustov, A.L. Tarasov, V.I. Bogdan, A.A. Tylov, J.W. Fulmer, Catal. Today 61 (2000) 123.
[29] S. Perathoner, F. Pino, G. Centi, G. Giordano, A. Katovic, J.B. Nagy, K. Lazar, P. Fejes, Studies Catal. Surf. Sci. 142 (2002) 503.
[30] J. Perez-Ramirez, M.S. Kumar, A. Brückner, J. Catal. 223 (2004) 13.
[31] S. Bordiga, R. Buzzoni, F. Geobaldo, C. Lamberti, E. Giamello, A. Zecchina, G. Leofanti, G. Petrini, G. Tozzolo, G. Vlaic, J. Catal. 158 (1996) 486.
[32] G. Lehmann, Z. Phys. Chem. Neue Folge 72 (1970) 279.
[33] N. Raffard-Pons y Moll, F. Banse, K. Miki, M. Nierlich, J.J. Girerd, Eur. J. Inorg. Chem. 8 (2002) 1941.
[34] R. Ganesan, B. Viswanathan, J. Molec. Catal. A: Chem. 181 (2002) 99.
[35] J. Glerup, K. Michelsen, N. Arulsamy, D.J. Hodgson, Inorg. Chim. Acta 274 (1998) 155.
[36] P.-P. Knops-Gerrits, A. Verberckmoes, R. Schoonheydt, M. Ichikawa, P.A. Jacobs, Micropor. Mesopor. Mater. 21 (1998) 475.
[37] X. Zhang, H. Furutachi, S. Fujinami, S. Nagatomo, Y. Maeda, Y. Watanabe, T. Kitagawa, M. Suzuki, JACS 127 (2005) 826.
[38] D. Wang, Z. Liu, F. Liu, X. Ai, X. Zhang, Y. Cao, J. Yu, T. Wu, Y. Bai, T. Li, X. Tang, Appl. Catal., A: Gen. 174 (1998) 25.
[39] J.J. Schneider, N. Czap, J. Hagen, J. Engstler, J. Ensling, P. Gutlich, U. Reinoehl, H. Bertagnolli, F. Luis, L. De Jongh, M. Wark, G. Grubert, G.L. Hornyak, R. Zanoni, Chem. Eur. J. 6 (2000) 4305.
[40] J.S. Jang, H.G. Kim, V.R. Reddy, S.W. Bae, S.M. Ji, J.S. Lee, J. Catal. 231 (2005) 213.
[41] M.S. Stave, J.B. Nicholas, J. Phys. Chem. 99 (1995) 15046.
[42] A. Chatterjee, A.K. Chandra, J. Molec. Catal. A: Chem. 119 (1997) 51.
[43] E. Hensen, Q. Zhu, P.-H. Liu, K.-J. Chao, R. van Santen, J. Catal. 226 (2004) 466.

[44] J. Dedecek, M. Tudor, J. Cejka, Studies Surf. Sci. Catal. 135 (2001) 1968.
[45] J.A. van Bokhoven, A.d.M.J. van der Eerden, D.C. Koningsberger, JACS 125 (2003) 7435.
[46] R. de Ruiter, K. Pamin, A.P.M. Kentgens, J.C. Jansen, H. van Bekkum, Zeolites 13 (1993) 611.
[47] R. De Ruiter, J.C. Jansen, H. Van Bekkum, Zeolites 12 (1992) 56.
[48] H. Kessler, J.M. Chezeau, J.L. Guth, H. Strub, G. Coudurier, Zeolites 7 (1987) 360.
[49] K. Yoshizawa, Y. Shiota, T. Kamachi, J. Phys. Chem. B 107 (2003) 11404.
[50] S.P. De Visser, S. Shaik, JACS 125 (2003) 7413.
[51] A.M. Ferretti, C. Oliva, L. Forni, G. Berlier, A. Zecchina, C. Lamberti, J. Catal. 208 (2002) 83.
[52] G. Berlier, G. Ricchiardi, S. Bordiga, A. Zecchina, J. Catal. 229 (2005) 127.